energies

MDPI

Article

Enhanced Thermoelectric Properties of Cu_3SbSe_4 Compounds via Gallium Doping

Degang Zhao *, Di Wu and Lin Bo

School of Materials Science and Engineering, University of Jinan, Jinan 250022, China; 18366100143@163.com (D.W.); mse_bolin@yeah.net (L.B.)

* Correspondence: mse_zhaodg@ujn.edu.cn; Tel.: +86-531-8276-7561

Received: 1 September 2017; Accepted: 26 September 2017; Published: 6 October 2017

Abstract: In this study, the *p*-type Ga-doped $Cu_3Sb_{1-x}Ga_xSe_4$ compounds were fabricated by melting, annealing, grinding, and spark plasma sintering (SPS). The transport properties of Ga-doped $Cu_3Sb_{1-x}Ga_xSe_4$ compounds were investigated. As Ga content increased, the hole concentration of $Cu_3Sb_{1-x}Ga_xSe_4$ compounds increased, which led to an increase in electrical conductivity. Meanwhile, the Seebeck coefficient of the $Cu_3Sb_{1-x}Ga_xSe_4$ compounds decreased as Ga content increased. The extra phonon scattering originating from Ga-doping effectively depressed the lattice thermal conductivity of the $Cu_3Sb_{1-x}Ga_xSe_4$ compounds. The ZT value of Cu_3SbSe_4 markedly improved, which is primarily ascribed to the depressed lattice thermal conductivity and the increased electrical conductivity. The highest ZT value for the $Cu_3Sb_{0.985}Ga_{0.015}Se_4$ compound was 0.54 at 650 K, which is two times higher than that of a pure Cu_3SbSe_4 compound.

Keywords: thermoelectric; Cu_3SbSe_4; gallium doping; spark plasma sintering

1. Introduction

With the global environmental issue and energy crisis becoming more and more serious, developing renewable and eco-friendly technologies for the sustainable development has gained more attention. Moreover, substantial amounts of waste heat from industrial, private, and transport sectors in modern society should be effectively recovered. Thermoelectric material provides a possibility to solve the issues mentioned above. Thermoelectric material is a kind of energy conversion material, which can realize the conversion between heat energy and electric energy. Thermoelectric material is expected to play a significant role in the field of electronic cooling, power generation, and waste heat recovery. The efficiency of thermoelectric material is usually characterized by the dimensionless figure of merit ZT. The ZT value can be calculated using the equation $ZT = \sigma\alpha^2 T/\kappa$, where κ, T, α, and σ are the total thermal conductivity, absolute temperature, Seebeck coefficient, and electrical conductivity, respectively [1–5]. The total thermal conductivity consists of a carrier part (κ_c) and a phonon part (κ_l). Therefore, a large ZT requires the thermoelectric material to have a low κ, a high α, and a high σ. Nowadays, developing high ZT material has been a research focus in the field of thermoelectric materials. As the α, σ, and κ_e of a material are associated closely with carrier concentration, how to optimize the carrier concentration to realize the maximum ZT is a key issue in this field. To improve ZT, many feasible methods have been developed and applied. Band engineering including electric band structure and valley degeneracy has been regarded as an efficient approach to improve the power factor (PF = $\alpha^2\sigma$), thereby enhancing the ZT. Doping or nanostructuring are also effective ways of enhancing the ZT by introducing extra phonon scattering centers [6–10].

Recently, copper-based chalcogenide semiconductors have attracted much attention because of their relatively high carrier mobility (μ_H) and low κ, such as CuGa(In)Te_2, Cu_2CdSnX_4 (X = Se, S), Cu_2SnSe_3, and Cu_3SbSe_4 [11–14]. Among these compounds, ternary Cu_3SbSe_4 semiconductor has

emerged as a promising thermoelectric material because of its narrow band gap and large carrier effective mass. Cu_3SbSe_4 has a superlattice of a zinc-blended structure and is of the type Cu_2FeSnS_4 with space group I-42m. The Cu/Se atoms form an electrically conductive framework and the remaining Sb atoms form the one- dimensional [$SbSe_4$] tetrahedra. This special tetrahedra in the Cu_3SbSe_4 crystal structure can enhance phonon scattering, similar to the "rattling atom" in skutterudite, resulting in a decrease in lattice thermal conductivity. Therefore, Cu_3SbSe_4 has a relatively low thermal conductivity. However, the electrical properties of intrinsic Cu_3SbSe_4 is poor due to its low hole concentration (p), which decreases the thermoelectric performance and leads to a low ZT value in the middle temperature range [15–18]. Theoretically, partial substitution on the Sb site of the Cu_3SbSe_4 can tune its electrical conductivity so as to enhance the thermoelectric performance. Previous studies about doping on the Sb site have been carried out, and some valuable work has been achieved [19,20]. Qin et al. synthesized the Al-doped $Cu_3Sb_{1-x}Al_xSe_4$ compounds and the maximum ZT reached 0.58 @ 600 K [21]. Similarly, Ge-doping or In-doping on the Sn site of Cu_3SbSe_4 was carried out, and the ZT value was enhanced to some extent [22,23]. Gallium has been shown to be a promising dopant in copper-based chalcogenide systems [24], but very little literature on Cu_3SbSe_4 has been reported. In the present work, the Ga substation on the Sb site is investigated in synthesized $Cu_3Sb_{1-x}Ga_xSe_4$ compounds, and our experimental results demonstrate that Ga-doping can effectively optimize carrier concentration (p) and decrease κ simultaneously. The paper investigated the phase composition, microstructure, and transport properties of $Cu_3Sb_{1-x}Ga_xSe_4$ compounds. The highest ZT of 0.54 was obtained for the $Cu_3Sb_{0.985}Ga_{0.015}Se_4$ compound.

2. Experimental Procedures

$Cu_3Sb_{1-x}Ga_xSe_4$ (x = 0, 0.005, 0.010, 0.015) compounds were conventionally synthesized via melting, annealing, grinding, and spark plasma sintering (SPS). The stoichiometric mixtures of pure elements Cu (powder, 99.98%), Sb (powder, 99.998%), Ga (granule, 99.998%), and Se (granule, 99.998%) were loaded in a graphite crucible. Then, the graphite crucible was sealed in a quartz tube, heated to 1173 K, and left for 720 min. The quartz tube was slowly cooled to 773 K at the rate of 0.5 K/min and subsequently quenched in salt water. Then, the sample was annealed at 573 K and the holding time is 48 h to ensure homogeneity. Lastly, the resultant alloys were ground in ethyl alcohol in an agate mortar. The obtained powder was sintered via SPS at 683 K in a vacuum of 0.1 Pa. The axial pressure and holding time were 50 MPa and 5 min, respectively. The Archimedes method was adopted to measure the density (d) of samples.

X-ray diffractometer equipment with Cu K_α radiation (Rigaku Rint 2000) was used to analyze the phase composition of the $Cu_3Sb_{1-x}Ga_xSe_4$ samples. Scanning electron microscopy (SEM, JXA-8200, JEOL, Tokyo, Japan) was employed to characterize the microstructure of $Cu_3Sb_{1-x}Ga_xSe_4$ samples. ZEM-3 apparatus (ULVAC-RIKO, Yokohama, Japan) was used to measure the σ and α in the temperature range of 300–650 K in an argon atmosphere. The measurement of thermal diffusivity (λ) of $Cu_3Sb_{1-x}Ga_xSe_4$ compounds was carried out using a laser flash equipment (Netzsch, LFA427) in an argon atmosphere under a vacuum of 0.001 Pa. A differential scanning calorimetry (Netzsch, DSC404, Munich, Germany) was used to measure the specific heat capacity (C_p) of $Cu_3Sb_{1-x}Ga_xSe_4$ compounds. The thermal conductivity was then obtained by the equation $\kappa = d\lambda C_p$. Van der Pauw's method was adopted to measure the Hall coefficient (R_H). Hall measurement was carried out in a vacuum of 0.1 Pa with a constant magnetic strength of 0.5 T. The p can be calculated using the equation $p_{\mathrm{H}} = 1/(R_H e)$, where e is the electron charge. The μ_H was obtained using the equations of $\mu_H = R_H\sigma$.

3. Results and Discussion

3.1. XRD Analysis and Microstructure

The X-ray diffraction patterns of $Cu_3Sb_{1-x}Ga_xSe_4$ ($0 \leq x \leq 0.015$) compounds is present in Figure 1. All major XRD peaks coincide well with the stand JCPDS card of Cu_3SbSe_4 (No. 01-085-0003). Therefore, the Ga-doped $Cu_3Sb_{1-x}Ga_xSe_4$ compounds are single phase and have the same crystallographic structure with a pure Cu_3SbSe_4 phase. In addition, no impurity phase was detected in the XRD results, suggesting the amount of Ga-doping in this study is within the doping limit. However, as the Ga content in $Cu_3Sb_{1-x}Ga_xSe_4$ increases, no obvious peak shift is found. On the one hand, the Ga content is very low; on the other hand, it is possibly related with the similar atomic radius of Ga and Sb. Chen et al. synthesized the $Cu_3Sb_{1-x}Ge_xSe_4$ compounds and the small atomic radius of Ge resulted in a decrease in the lattice constant of the $Cu_3Sb_{1-x}Ge_xSe_4$ compounds [22]. The SEM image and elemental distribution maps, including Cu, Sb, and Se elements for the $Cu_3Sb_{0.985}Ga_{0.015}Se_4$ compound is displayed in Figure 2. It can be seen that each element (Cu, Sb and Se) was uniform with no notable brighter regions, indicating that all elements distributed homogeneously in the matrix. Meanwhile, no visible other phase can be found in the SEM, which is also in agreement with the XRD result above.

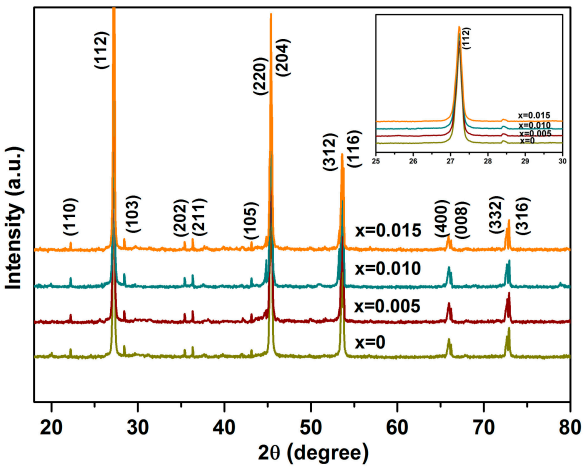

Figure 1. XRD patterns of Ga-doped $Cu_3Sb_{1-x}Ga_xSe_4$ ($0 \leq x \leq 0.015$) compounds.

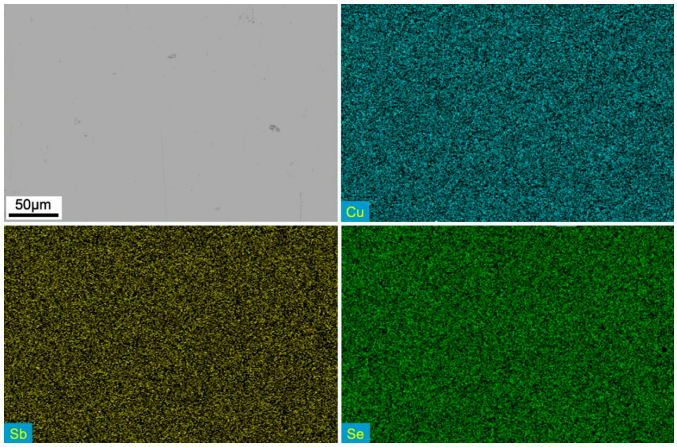

Figure 2. SEM image and elemental distribution maps of $Cu_3Sb_{0.985}Ga_{0.015}Se_4$ compounds.

3.2. Electrical Performance

The temperature dependence of σ for the $Cu_3Sb_{1-x}Ga_xSe_4$ ($0 \leq x \leq 0.015$) compounds is present in Figure 3. As the temperature increases, the σ of the $Cu_3Sb_{1-x}Ga_xSe_4$ samples increases, indicating typical heavily doped semiconducting behavior. Moreover, the σ of these samples increases as the Ga content increases. The improvement in σ for $Cu_3Sb_{1-x}Ga_xSe_4$ should be ascribed to an increase in carrier concentration (p) resulting from the Ga-doping. The calculated carrier concentration of pure Cu_3SbSe_4 was about 1.90×10^{18} cm^{-3}. The thermoelectric properties and structural parameters of $Cu_3Sb_{1-x}Ga_xSe_4$ compounds at room temperature are listed in Table 1. The hole concentration of Ga-doped $Cu_3Sb_{1-x}Ga_xSe_4$ is higher than that of pure Cu_3SbSe_4. The hole concentration increases rapidly from 1.90×10^{18} to 12.7×10^{18} cm^{-3} when the Ga content increases from 0 to 0.015. Meanwhile, the corresponding μ_H decreases from 76.2 cm^2/Vs for pure Cu_3SbSe_4 to 30.8 cm^2/Vs for the $Cu_3Sb_{0.985}Ga_{0.015}Se_4$ sample. The extra ionized impurity scattering and alloy scattering should result in a decrease in μ_H. The μ_H of the $Cu_3Sb_{1-x}Ga_xSe_4$ ($0 \leq x \leq 0.015$) compounds is present in Figure 4. It can be seen that the μ_H of these compounds shows a gradual downward trend with the increase in temperature. In addition, the relationship of $\mu_H \infty T^{-3/2}$ can be found at high temperature, which indicates that the dominant scattering mechanism of $Cu_3Sb_{1-x}Ga_xSe_4$ ($0 \leq x \leq 0.015$) compounds is phonon scattering. As the Ga content increases, the relationship of $\mu_H \infty T^{-3/2}$ of these compounds becomes weak, indicating that the dominant mechanism is mixed scattering for the $Cu_3Sb_{1-x}Ga_xSe_4$ compounds at high temperature [8]. Moreover, the μ_H of Ga-doped $Cu_3Sb_{1-x}Ga_xSe_4$ samples in this study is between 30 and 40 cm^2 V^{-1} s^{-1} at room temperature. Shi et al. calculated the μ_H of Cu_2SnSe_3 materials, and the results showed that the μ_H was about 52 cm^2 V^{-1} s^{-1} at room temperature. The similar Hall mobility is possibly related to the similar density of states effective mass [25,26].

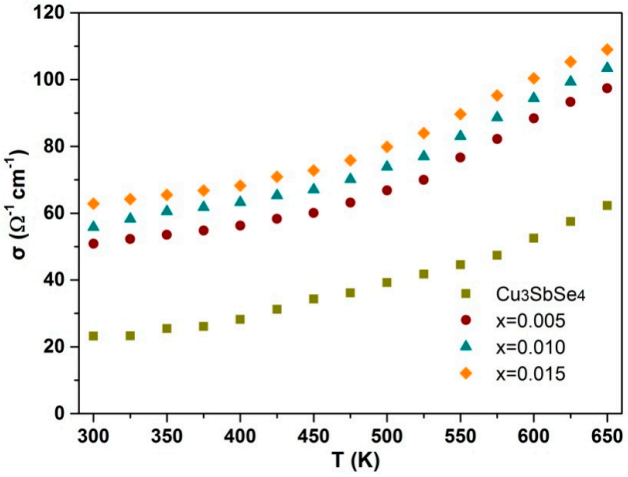

Figure 3. Electrical conductivity of $Cu_3Sb_{1-x}Ga_xSe_4$ ($0 \leq x \leq 0.015$) compounds.

Table 1. Thermoelectric properties and structural parameter of Ga-doped $Cu_3Sb_{1-x}Ga_xSe_4$ ($0 \leq x \leq 0.015$) compounds at room temperature.

x	κ_L (W m^{-1} K^{-1})	Relative Density	α (μV/K)	σ (Ω^{-1} cm^{-1})	p (10^{18} cm^{-3})	μ_H (cm^2/Vs)	m^* (m_0)
0	3.19	98.5%	405	23.2	1.90	76.2	1.2
0.005	2.71	98.7%	244	50.8	8.01	39.2	1.4
0.010	2.54	98.3%	222	55.9	9.84	35.5	1.6
0.015	2.29	98.8%	208	62.7	12.7	30.8	1.5

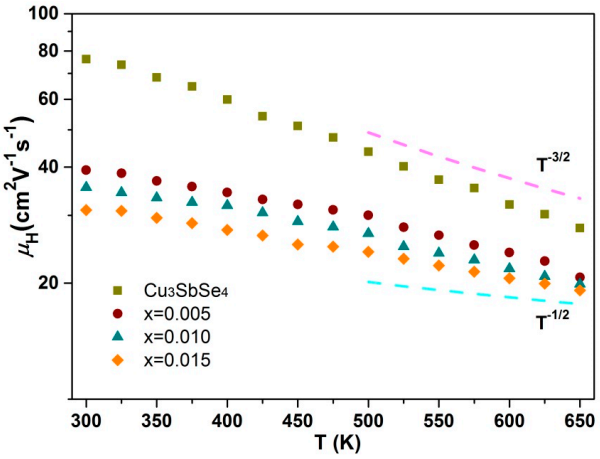

Figure 4. Carrier mobility of $Cu_3Sb_{1-x}Ga_xSe_4$ ($0 \leq x \leq 0.015$) compounds.

Figure 5 demonstrates the Seebeck coefficients for $Cu_3Sb_{1-x}Ga_xSe_4$ ($0 \leq x \leq 0.015$) compounds. All of the $Cu_3Sb_{1-x}Ga_xSe_4$ samples exhibit a *p*-type character, and the major charge carriers are holes. As the temperature increases, the α of the pure Cu_3SbSe_4 samples decreases, from 405 μV/K at 300 K to 291 μV/K at 650 K. Nevertheless, the α of Ga-doped samples firstly increases approximately linearly to a maximum value, and then decreases, suggesting a heavily degenerate semiconductor behavior. For example, the peak value of α for the $Cu_3Sb_{0.985}Ga_{0.015}Se_4$ compound is 295 μV/K at 500 K. The α decreases linearly to 260 μV/K at 650 K. Similar behaviors have been reported in In-doped Cu_3SbSe_4 samples [26]. In addition, the α of Ga-doped samples decreases as the Ga-doped content increases because of the increase in hole concentration. Generally, the Seebeck coefficient can be written as:

$$\alpha = \pm\frac{k_B}{e}\left[2 + \ln\frac{2(2\pi m^* k_B T)^{\frac{3}{2}}}{h^3 p}\right] \quad (1)$$

where m^* is the density of states effective mass, h is Planck's constant, and k_B is Boltzmann constant [4–6]. As the increase in hole concentration has a more significant effect than the increase in the density of states effective mass (m^*, Table 1), the α of the Ga-doped $Cu_3Sb_{1-x}Ga_xSe_4$ compounds decreases as Ga-doped content increases.

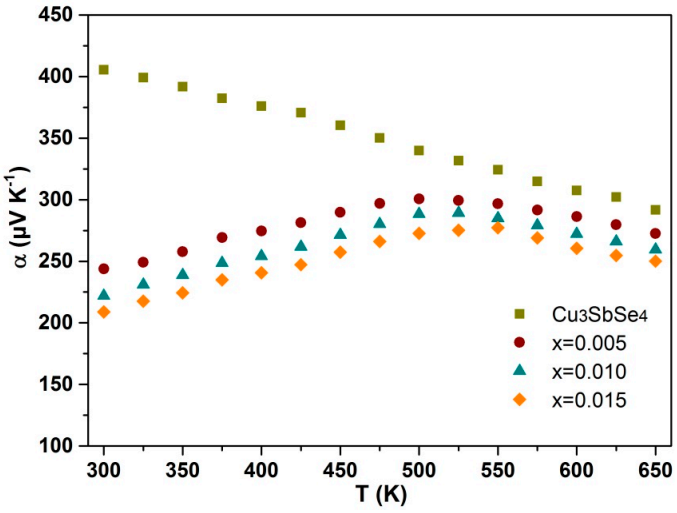

Figure 5. Seebeck coefficient of $Cu_3Sb_{1-x}Ga_xSe_4$ ($0 \leq x \leq 0.015$) compounds.

3.3. Thermal Conductivity

Figure 6a,b show the temperature dependences of the total thermal conductivity κ and the phonon part κ_l for $Cu_3Sb_{1-x}Ga_xSe_4$ ($0 \leq x \leq 0.015$) compounds, respectively. The κ of all $Cu_3Sb_{1-x}Ga_xSe_4$ compounds decreases as the temperature increases. In addition, the κ of Ga-doped $Cu_3Sb_{1-x}Ga_xSe_4$ samples is markedly lower that of pure Cu_3SbSe_4, which should be attributed to the decrease in κ_l, resulting from the increase of point defect scattering. The κ of the material consists of a carrier part (κ_c) and a lattice part (κ_l). The electron part (κ_c) can be obtained using the Wiedemann–Franz equation, $\kappa_c = L_0\sigma T$, where L_0 is the Lorenz number. As the Lorenz number varies with the temperature and the composition of materials, the precise Lorenz number is adopted according to the method in [27]. Therefore, the κ_l can be obtained by subtracting the κ_c from the κ. The κ_l of Ga-doped $Cu_3Sb_{1-x}Ga_xSe_4$ compounds drastically decreases with increasing Ga content, as shown in Figure 6b. In addition, the κ_l shows a temperature dependence of T^{-1}, as illustrated by the blue dotted line, indicating that phonon–phonon scattering is the dominant scattering for the pure Cu_3SbSe_4 sample and the Ga-doped $Cu_3Sb_{1-x}Ga_xSe_4$ samples. For the $Cu_3Sb_{0.985}Ga_{0.015}Se_4$ sample, the κ_l is 2.27 W/mK at room temperature, which is reduced by 30% than that of pure Cu_3SbSe_4. The minimum κ_l of the $Cu_3Sb_{0.985}Ga_{0.015}Se_4$ sample in this study is 0.62 W/mK at 650K. As far as is known, the theoretical minimal value of lattice thermal conductivity, κ_{lmin}, can be evaluated according to the equation $\kappa_{lmin} = 1/3lv_mC_v$, where l, C_v, and v_m are the mean free path of the phonon, the isochoric specific heat, and the mean sound velocity, respectively. The red dashed line in Figure 6b presents the theoretical minimal value of lattice thermal conductivity for pure Cu_3SbSe_4 and the obtained κ_{lmin} is 0.47 W m^{-1} K^{-1}, as shown in the red dashed line. It also can be concluded from Figure 6b that there is still a potential possibility to further decrease the κ_l of the Cu_3SbSe_4 compound.

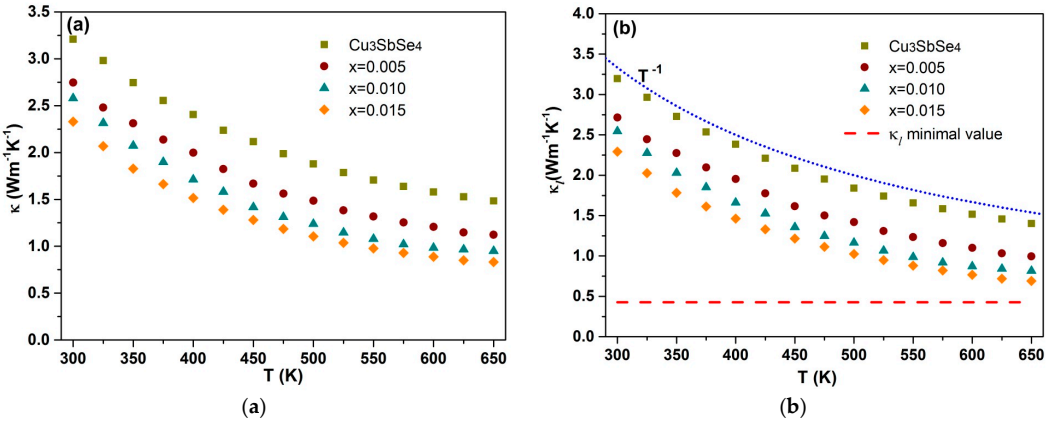

Figure 6. (**a**) Total thermal conductivity (κ) and (**b**) lattice thermal conductivity (κ_l) for $Cu_3Sb_{1-x}Ga_xSe_4$ ($0 \leq x \leq 0.015$) compounds. The blue dotted line represents the κ_l-T^{-1}. Red dashed line shows the theoretical minimal value of lattice thermal conductivity for pure Cu_3SbSe_4.

3.4. Figure of Merit

The ZT value for $Cu_3Sb_{1-x}Ga_xSe_4$ ($0 \leq x \leq 0.015$) compounds is present in Figure 7. The ZT value of Cu_3SbSe_4 sample increases from 0.02 to 0.18 in the temperature ranged from room temperature to 650 K. Compared with the ZT value of pure Cu_3SbSe_4, the ZT of Ga-doped $Cu_3Sb_{1-x}Ga_xSe_4$ sample is obviously improved. For example, the ZT of the $Cu_3Sb_{0.995}Ga_{0.005}Se_4$ compound is 0.36 at 650 K, which is one higher than the ZT of pure Cu_3SbSe_4. The maximal ZT value of the $Cu_3Sb_{0.985}Ga_{0.015}Se_4$ compound can reach 0.54 at 650 K, which is about 3 times as large as that of the pure Cu_3SbSe_4 compound.

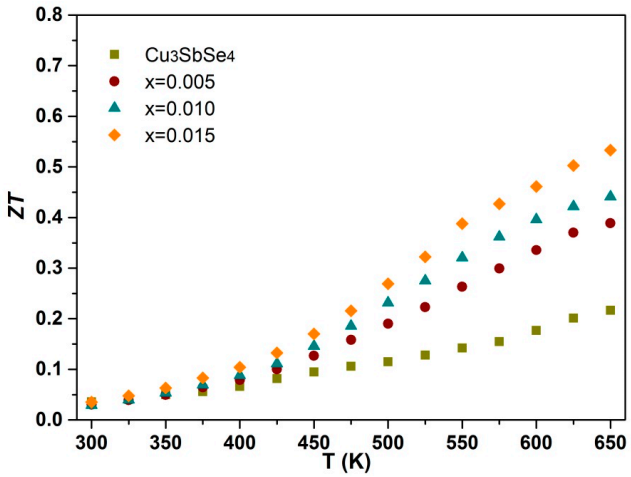

Figure 7. Thermoelectric dimensionless figure of merit (ZT) for $Cu_3Sb_{1-x}Ga_xSe_4$ ($0 \leq x \leq 0.015$) compounds.

4. Conclusions

In this study, *p*-type Ga-doped $Cu_3Sb_{1-x}Ga_xSe_4$ compounds were fabricated by melting, annealing, and SPS. Compared with a pure Cu_3SbSe_4 compound, Ga-doped $Cu_3Sb_{1-x}Ga_xSe_4$ compounds showed a large increase in electrical conductivity resulting from the substantial increase in carrier concentration. However, the Seebeck coefficient of the $Cu_3Sb_{1-x}Ga_xSe_4$ compounds decreased as the Ga content increased. The Seebeck coefficient of Ga-doped samples firstly increased approximately linearly to a maximum value and then decreased. Meanwhile, the thermal conductivity of the $Cu_3Sb_{1-x}Ga_xSe_4$ compounds markedly decreased because of the extra phonon scattering originating from the Ga-doping on the Sb site. Therefore, the increased electrical conductivity and the depressed lattice thermal conductivity effectively enhanced the ZT value of Cu_3SbSe_4. The maximum ZT value for the $Cu_3Sb_{0.985}Ga_{0.015}Se_4$ compounds was 0.54 at 650 K, which is around two times larger than that of pure Cu_3SbSe_4 compounds.

Acknowledgments: We would like to thank the help for the measurement of thermal conductivity in Tongji University, China. This work was supported by the National Natural Science Foundations of China (No. 51772132 and No. 51471076).

Author Contributions: All authors contributed to the material synthesis, measurement, data analysis, and correction of the manuscript. The design of experiment and data analysis was performed by Degang Zhao. The experiments and measurement was carried out by Di Wu and Lin Bo. The paper was written by Degang Zhao.

Conflicts of Interest: The authors declare no conflicts of interest.

References

1. Snyder, G.J.; Toberer, E.S. Complex thermoelectric materials. *Nat. Mater.* **2008**, *7*, 105–114. [CrossRef] [PubMed]
2. Pei, Y.Z.; Shi, X.Y.; LaLonde, A.; Wang, H.; Chen, L.D.; Snyder, G.J. Convergence of electronic bands for high performance bulk thermoelectric. *Nature* **2011**, *473*, 66–69. [CrossRef] [PubMed]
3. Pei, Y.Z.; Wang, H.; Snyder, G.J. Band Engineering of Thermoelectric Materials. *Adv. Mater.* **2012**, *24*, 6125–6135. [CrossRef] [PubMed]
4. Hong, M.; Chen, Z.G.; Pei, Y.Z.; Yang, L.; Zou, J. Limit of ZT enhancement in rocksalt structured chalcogenides by band convergence. *Phys. Rev. B* **2016**, *94*, 16120. [CrossRef]
5. Hong, M.; Chen, Z.G.; Yang, L.; Zou, J. $Bi_xSb_{2-x}Te_3$ nanoplates with enhanced thermoelectric performance due to sufficiently decoupled electronic transport properties and strong wide-frequency phonon scatterings. *Nano Energy* **2016**, *20*, 144–155.

6. Fitriani, R.O.; Long, B.D.; Barma, M.C.; Riaz, M.; Sabri, M.F.; Said, S.M.; Saidur, R. A review on nanostructures of high temperature thermoelectric materials for waste heat recovery. *Renew. Sustain. Energy Rev.* **2016**, *64*, 635–659. [CrossRef]
7. Lu, N.D.; Li, L.; Liu, M. A review of carrier thermoelectric-transport theory in organic semiconductors. *Phys. Chem. Chem. Phys.* **2016**, *18*, 19503–19525. [CrossRef] [PubMed]
8. Hong, M.; Chasapis, T.C.; Chen, Z.G.; Yang, L.; Kanatzidis, M.G.; Snyder, G.J.; Zou, J. N-type $Bi_2Te_{3-x}Se_x$ Nanoplates with enhanced thermoelectric efficiency driven by wide-frequency phonon scatterings and synergistic carrier scatterings. *ACS Nano* **2016**, *10*, 4719–4727. [CrossRef] [PubMed]
9. Hong, M.; Chen, Z.G.; Yang, L.; Zou, J. Enhancing thermoelectric performance of Bi_2Te_3-based nanostructures through rational structure design. *Nanoscale* **2016**, *8*, 8681–8686. [CrossRef] [PubMed]
10. Hong, M.; Chen, Z.G.; Yang, L.; Chasapis, T.C.; Kang, S.D.; Zou, Y.C.; Auchterlonie, G.J.; Kanatzidis, M.G.; Snyder, G.J.; Zou, J. Enhancing the thermoelectric performance of $SnSe_{1-x}Te_x$ nanoplates through band engineering. *J. Mater. Chem. A* **2017**, *5*, 10713–10721.
11. Kosuga, A.; Plirdpring, T.; Higashine, R.; Matsuzawa, M.; Kurosaki, K.; Yamanaka, S. High temperature thermoelectric properties of $Cu_{1-x}InTe_2$ with a chalcopyrite structure. *Appl. Phys. Lett.* **2012**, *100*, 042108. [CrossRef]
12. Zeier, W.G.; Pei, Y.Z.; Pomrehn, G.; Day, T.; Heinz, N.; Heinrich, C.P.; Snyder, G.J.; Tremel, W. Phonon scattering through a local anisotropic structural disorder in the thermoelectric solid solution $Cu_2Zn_{1-x}Fe_xGeSe4$. *J. Am. Chem. Soc.* **2013**, *135*, 726–732. [CrossRef] [PubMed]
13. Fan, F.J.; Yu, B.; Wang, Y.X.; Zhu, Y.L.; Liu, X.J.; Yu, S.H.; Ren, Z.F. Colloidal synthesis of $Cu_2CdSnSe_4$ nanocrystals and hot pressing to enhance the thermoelectric figure of merit. *J. Am. Chem. Soc.* **2011**, *133*, 15910–15913. [CrossRef] [PubMed]
14. Skoug, E.J.; Cain, J.D.; Majsztrik, P.; Kirkham, M.; Morelli, D.T. Doping effects on the thermoelectric properties of Cu_3SbSe_4. *Sci. Adv. Mater.* **2011**, *3*, 602–606. [CrossRef]
15. Wei, T.R.; Wang, H.; Gibbs, Z.M.; Wu, C.F.; Snyder, G.J.; Li, J.F. Thermoelectric properties of Sn-doped p-type Cu_3SbSe_4: A compound with large effective mass and small band gap. *J. Mater. Chem. A* **2014**, *2*, 13527–13533. [CrossRef]
16. Yang, C.Y.; Huang, F.Q.; Wu, L.M.; Xu, K. New stannite-like p-type thermoelectric material Cu_3SbSe_4. *J. Phys. D Appl. Phys.* **2011**, *44*, 295404. [CrossRef]
17. Suzumura, A.; Watanabe, M.; Nagasako, N.; Asahi, R. Improvement in thermoelectric properties of Se-free Cu_3SbSe_4 compound. *J. Electron. Mater.* **2014**, *43*, 2356–2360. [CrossRef]
18. Li, X.Y.; Li, D.; Xin, H.X.; Zhang, J.; Song, C.J.; Qin, X.Y. Effects of bismuth doping on the thermoelectric properties of Cu_3SbSe_4 at moderate temperature. *J. Alloys Compd.* **2013**, *561*, 105–108. [CrossRef]
19. Kumar, A.; Dhama, P.; Saini, D.S.; Banerji, P. Effects of Zn substitution at a Cu site on the transport behavior and thermoelectric properties in Cu_3SbSe_4. *RSC Adv.* **2016**, *6*, 5528–5534. [CrossRef]
20. Li, D.; Li, R.; Qin, X.Y.; Song, C.J.; Xin, H.X.; Zhang, J.; Guo, G.L.; Zou, T.H.; Zhu, X.G. Co-precipitation synthesis of nanostructured Cu_3SbSe_4 and its Sn-doped sample with high thermoelectric performance. *Dalton Trans.* **2014**, *43*, 1888–1896. [CrossRef] [PubMed]
21. Li, Y.Y.; Qin, X.Y.; Li, D.; Li, X.Y.; Liu, Y.F.; Zhang, J.; Song, C.J.; Xin, H.X. Transport properties and enhanced thermoelectric performance of aluminum doped Cu_3SbSe_4. *RSC Adv.* **2015**, *5*, 31399–31403. [CrossRef]
22. Chang, C.H.; Chen, C.L.; Chiu, W.T.; Chen, Y.Y. Enhanced thermoelectric properties of Cu_3SbSe_4 by germanium doping. *Mater. Lett.* **2017**, *186*, 227–230. [CrossRef]
23. Dan, Z.; Yang, J.Y.; Jiang, Q.H.; Fu, L.W.; Xiao, Y.; Zhou, Z.W. Improvement of thermoelectric properties of Cu_3SbSe_4 compound by In doping. *Mater. Des.* **2016**, *98*, 150–154.
24. Zhang, J.; Qin, X.Y.; Li, D.; Xin, H.X.; Song, C.J.; Li, L.L.; Zhu, X.G.; Wang, Z.M.; Wang, L. Enhanced thermoelectric performance of $CuGaTe_2$ based composites incorporated with nanophase Cu_2Se. *J. Mater. Chem. A* **2014**, *2*, 2891–2985. [CrossRef]
25. Zhao, D.G.; Ning, J.A.; Wu, D.; Zuo, M. Enhanced thermoelectric performance of Cu_2SnSe_3 based composites incorporated with nano-fullerene. *Materials* **2016**, *9*, 629. [CrossRef] [PubMed]

26. Shi, X.Y.; Huang, F.Q.; Liu, M.L.; Chen, L.D. Thermoelectric properties of tetrahedrally bonded wide gap stannite compounds $Cu_2ZnSn_{1-x}In_xSe_4$. *J. Am. Chem. Soc.* **2009**, *94*, 122103. [CrossRef]
27. Kim, H.S.; Gibbs, Z.M.; Tang, Y.L.; Wang, H.; Snyder, G.J. Characterization of Lorenz number with Seebeck coefficient measurement. *APL Mater.* **2015**, *3*, 041506. [CrossRef]